Electronic Supplementary Material (ESI) for Nanoscale Advances.

Supplementary Information:

Antimicrobial Peptide-conjugated phage-mimicking nanoparticles exhibit potent antibacterial action against *Streptococcus pyogenes* in murine wound infection models

Johanna Olesk[a], Deborah Donahue[b], Jessica Ross[c], Conor Sheehan[d], Zach Bennett[a], Kevin Armknecht[e], Carlie Kudary[f], Juliane Hopf[f], Victoria A. Ploplis[b], Francis J. Castellino[b], Shaun W. Lee[c] and Prakash D. Nallathamby[*a,f]

[a] *Dept. of Aerospace and Mechanical Engineering, University of Notre Dame, Notre Dame, Indiana, USA.*
[b] *W. M. Keck Center for Transgene Research, University of Notre Dame, Notre Dame, Indiana, USA.*
[c] *Dept. of Biological Sciences, University of Notre Dame, Notre Dame, Indiana, USA.*
[d] *Dept. of Chemistry and Biochemistry, University of Notre Dame, Notre Dame, Indiana, USA.*
[e] *Dept. of Pre-Professional Studies, University of Notre Dame, Notre Dame, Indiana, USA.*
[f] *Berthiaume Institute for Precision Health, University of Notre Dame, Notre Dame, Indiana, USA.*
[*]Corresponding Author: Email: pnallath@nd.edu; Tel: +1 574 631 7868

A. ICP-OES analysis on the nanoparticles.

ICP-OES analysis (ref. Main Manuscript Section 3.1) was carried out after each step of the synthesis, on SiO_2NPs, SiO_2AuNPs and PhaNPs without Syn71 modification, to quantitatively determine the presence of each element (Si, Au, Ag) on the nanoparticles after each synthesis step (Table S1). As expected, it was seen that the Si content was the highest on every nanoparticle variant (7.371, 3. 829 and 12.068 mg/ml for SiO_2NPs, SiO_2AuNPs and PhaNPs, respectively). No Au and Ag was detected in the SiO_2NP sample. SiO_2AuNP sample contained 0.174 mg/ml of Au while no Ag was detected, proving that the corresponding synthesis strep was successful. PhaNPs contained both, Au and Ag, 0.064 mg/ml and 3.924 mg/ml, respectively, confirming that our synthesis was successful.

Table S1 ICP-OES of nanoparticles at different synthesis steps to quantitatively confirm the presence of the expected elements.

	Si (mg/ml)	Au (mg/ml)	Ag (mg/ml)
SiO_2NP	7.371	0	0
SiO_2AuNP	3.829	0.124	0
PhaNPs	12.068	0.054	3.924

B. DLS/Zeta potential on the nanoparticles.

DLS analysis was carried out to study the behavior of the nanoparticles in solution (Main Manuscript Section 3.1). PhaNPs displayed hydrodynamic radius of the nanoparticles in solution with the average size of 781.7±498.5 nm (Table S2). PhaNP@Syn71 showed a diameter of 2582±641.2 nm, confirming the Syn71 peptide's successful conjugation to the nanoparticles, as well as a higher hydrodynamic radius than that of the unmodified PhaNPs. Zeta potential analysis revealed the change in surface potential after Syn71 peptide modification. The zeta potential of PhaNPs without Syn71 peptide modification was -16.0 mV with a conductivity of 17.8 mS/cm (Figure S1). The results for the modified PhaNP@Syn71, however, had an increased zeta potential of -8.54 mV with a conductivity of 16.8 mS/cm. Therefore, it was confirmed that the Syn71 modification was successful as the surface potential changed.

Table S2 DLS/Zeta potential table

	Size (nm)	Std. Dev (nm)	Zeta Potential (mV)	Conductivity (mS/cm)	Polydispersity index
PhaNPs	781.7	498.5	-16.0	17.8	0.261
PhaNP@Syn71	2582	641.2	-8.54	16.8	0.094
SiO_2AuNP	NA	NA	-9.21	17.8	NA
Syn71 peptide	NA	NA	-7.15	21.0	NA

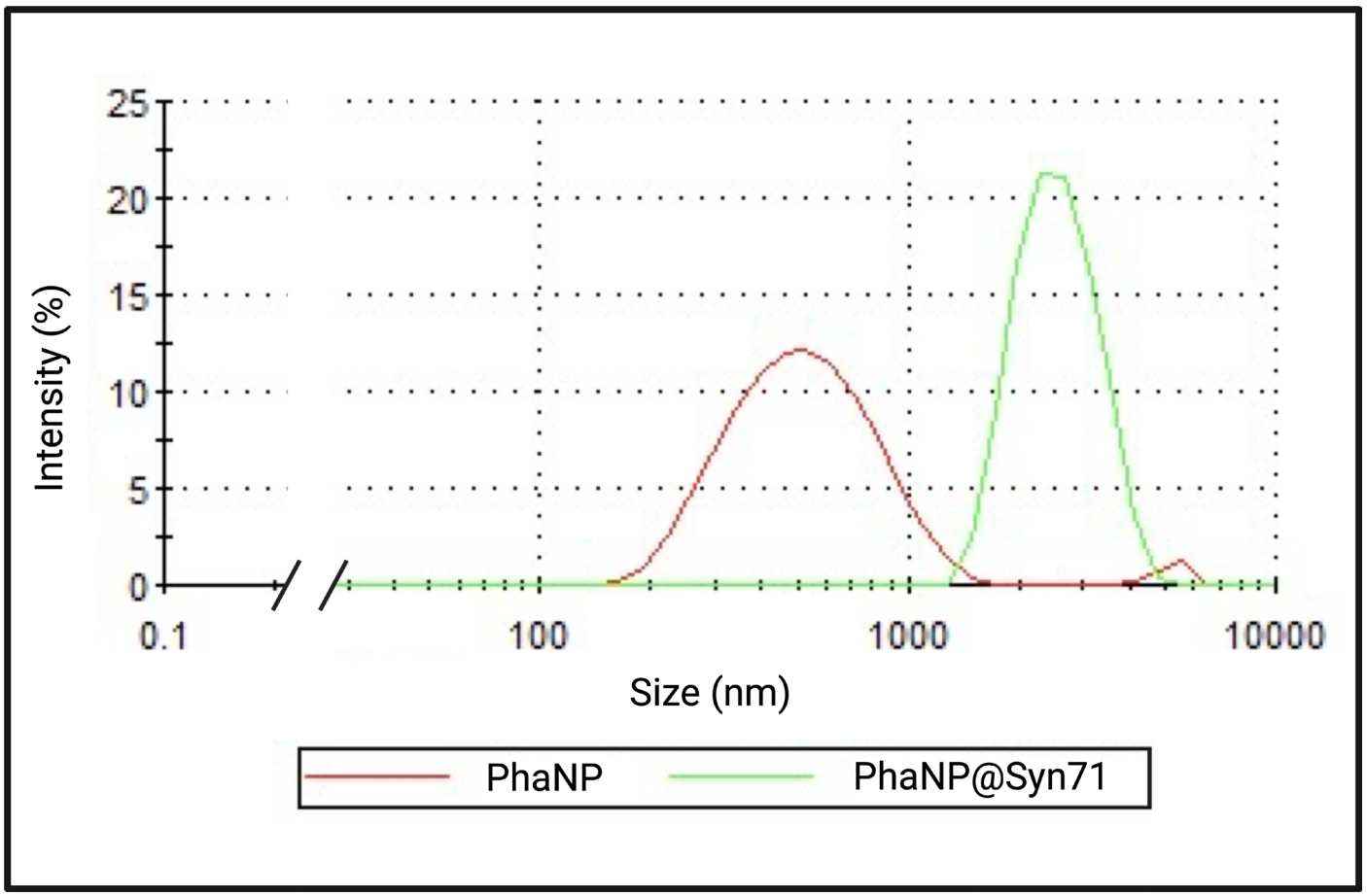

Fig. S1 DLS size distribution analysis on PhaNPs and PhaNP@Syn71.

C. LC-MS results of PhaNP@Syn71 supernatant in reference to Syn71 peptide standard.

LC-MS analysis was carried out on the supernatant samples collected from the PhaNP@Syn71 synthesis to confirm the degree of conjugation of Syn71 peptide on PhaNPs (Main Manuscript Section 3.1). The results showed no residual Syn71 peptide present in supernatant 1 (collected after the first spin-down), neither in supernatant 2 (collected after the wash and the second spin-down) compared to the standard of Syn71 peptide (Figure S2). Therefore, it was confirmed that all the peptide added to the PhaNPs during the synthesis of PhaNP@Syn71 had been chemisorbed onto the PhaNPs.

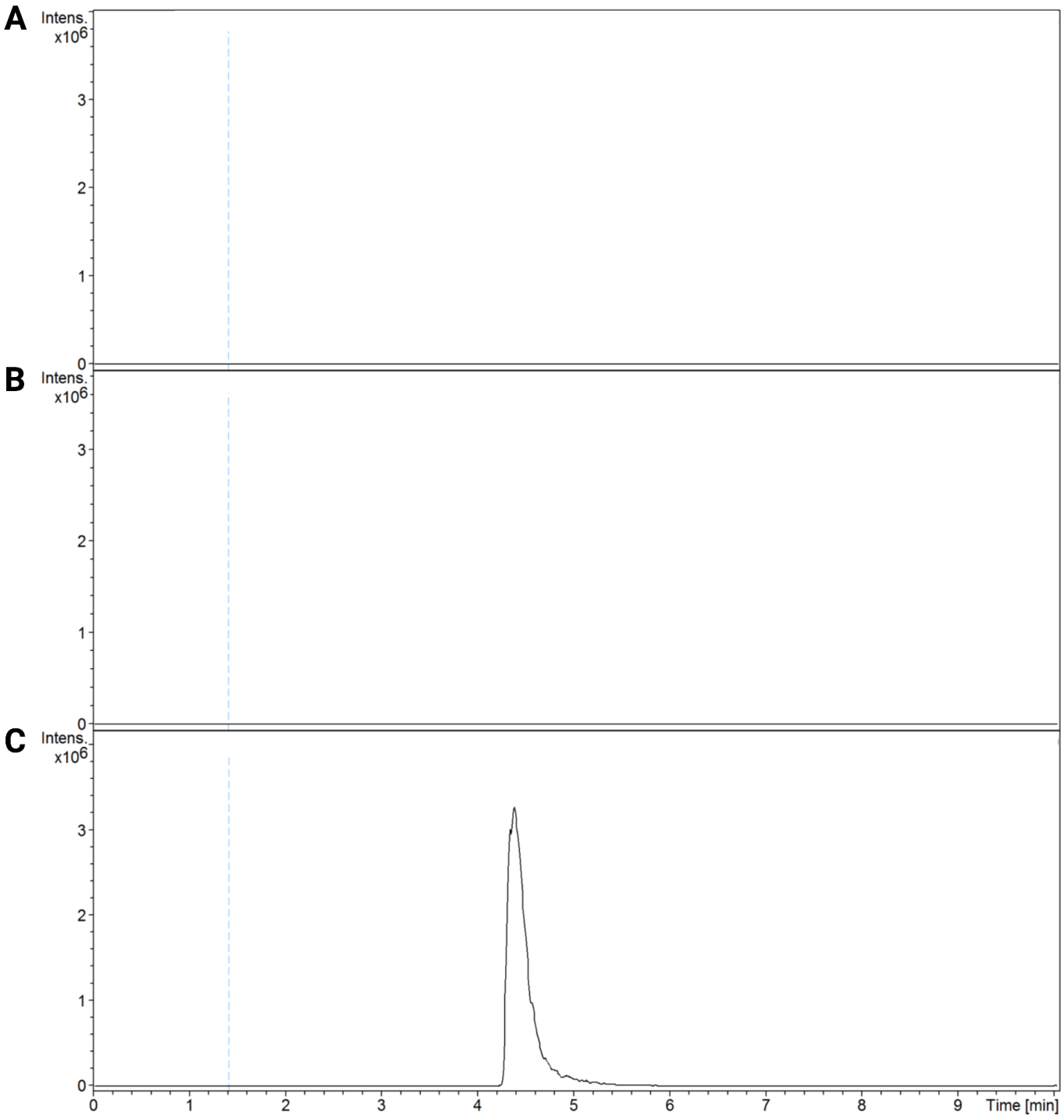

Fig. S2 The extracted-ion chromatograms of (A) supernatant 1, (B) supernatant 2, and (C) standard of Syn71.

D. Scratch closure assay scratch diameter change in time.

A scratch closure assay was carried out on the HaCaT cell line to study the cell migration in 24 h when incubated with Syn71 peptide as well as the PhaNP@Syn71 (Main Manuscript Section 3.2.1). The results indicated that while Syn71 did not hinder the scratch closure, there was no visible cell migration in cells incubated with any of the nanoparticle variants (SiO_2AuNPs, PhaNPs and PhaNP@Syn71) (Figure S3). This is due to the negative charge of the nanoparticles, which leads to their attachment onto the slide, preventing cell attachment.

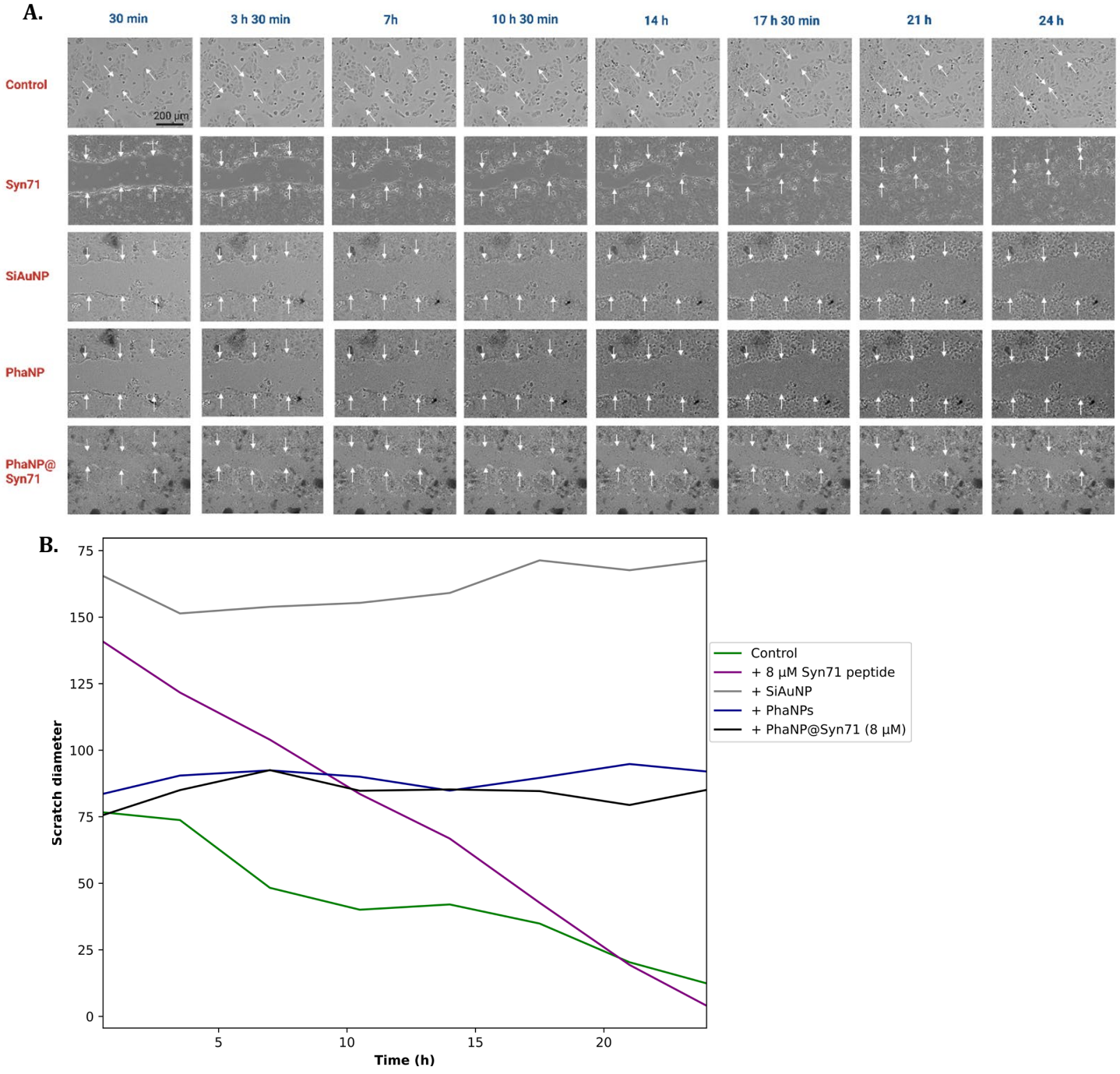

Fig. S3 (A) Representative longitudinal images of cell migration in control and test samples. **(B)** The Scratch closure assay scratch diameter change vs time was plotted. While the Syn71 peptide did not hinder or promote scratch closure, all the nanoparticle variants hindered HaCaT cell migration. We hypothesize this is because of the negatively charged nanoparticles binding to the positively tissue culture surface and thereby changing the tissue culture promoting nature of the original surface.

E. *In Vitro* Testing of Fixed *S. pyogenes* with thiol blocking Maleimide dyes to understand how PhaNPs are interreacting with bacterial membranes before disrupting bacterial membrane.

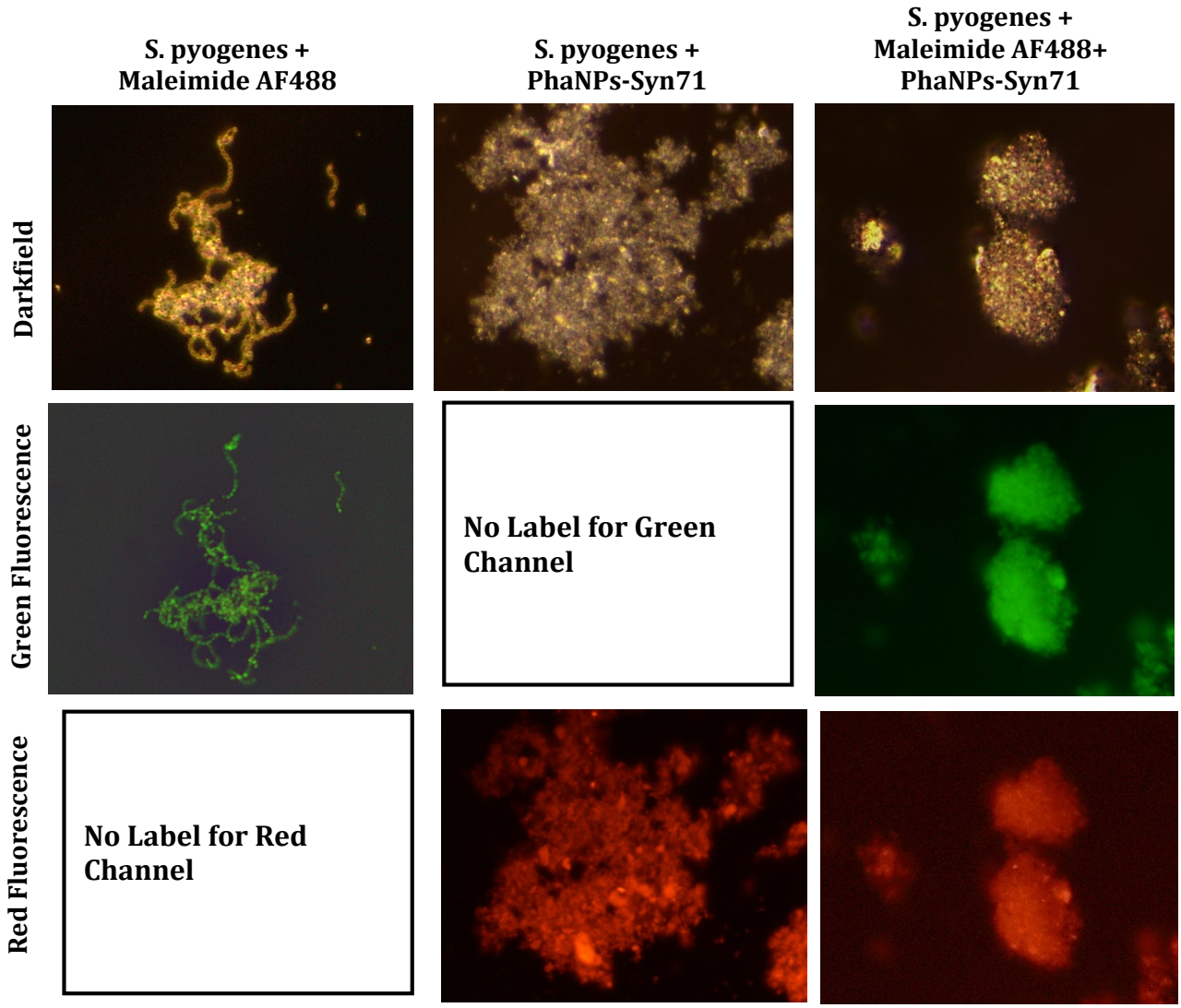

Figure S4*: Streptococcus pyogenes* was grown in LB media for 16 hours. The bacteria were pelleted and fixed in 4% buffered para-formaldehyde for 1 hour. Then bacteria were pelleted by centrifugation and resuspended in 1xPBS. Three test groups were formed to see if thiol residues on bacterial membrane were the points of contact before disruption of bacteria by PhaNPs.(a) Group 1: The OD_{600nm} was adjusted to 0.05 using 1x PBS for the fixed *S. pyogenes* bacteria. The 5mg/mL Af488-maleimide dye was diluted 100-fold by direct addition to the OD_{600nm} =0.05 bacteria solution. The solution was mixed by shaking in the fridge for 12 hours. The bacteria were rinsed thrice by centrifugation and then resuspended in 1X PBS. 10 microliters of the sample were dropped on a glass slide and imaged using dark-field microscopy and a 40X objective. Green fluorescence imaging clearly showed AF488-Maleimide staining of the fixed bacteria, which indicated the presence of thiol residues on the bacterial membrane. The maleimide group reacts specifically with sulfhydryl groups when the pH of the reaction mixture is between 6.5 and 7.5; the result is formation of a stable thioether linkage that is not reversible (i.e., the bond cannot be cleaved with reducing agents). We did not reduce any disulfide bridges, so those stayed intact. Maleimide staining and darkfield imaging confirmed the presence of the characteristic chain like structures of the *S.pyogenes*. (b) Group 2: The OD_{600nm} was adjusted to 0.05 using 1x PBS for the fixed *S. pyogenes* bacteria. Red fluorescent silica@Au NPs were synthesized using volume labeling techniques developed in our lab to incorporate rhodamine into the silica core[1, 2]. Red fluorescent silica@Au was added to OD_{600nm} = 0.05 adjusted *S. pyogenes* solution to a final silica@Au concentration of 0.2% v/v. Silica@Au was utilized as SEM images **(Figure.4B)** had confirmed that Silica@Au/Ag breaks down bacteria structure but Silica@Au does not breakdown bacteria completely thus giving us an insight into mode of interaction of the PhaNPs with the bacterial membrane. Interestingly dark field imaging and red fluorescence imaging revealed the lack of chain-like bacterial structures in the presence of silica@Au NPs. Instead, the bacteria were disjointed and present as clumps and red fluorescent silica@Au NPs were co-localized with the bacterial clumps. (c) Group 3: We took bacteria pre-treated with maleimide to block cysteine residues. We then added red fluorescent silica@Au NPs to a final concentration of 0.2% v/v. Interestingly dark field imaging and red fluorescence imaging again

revealed the lack of chain-like bacterial structures.

These experiments would indicate that *S.pyogenes* form chain like structures utilizing molecules that are not essentially thiol-rich. A brief literature survey turned up that Protein H is a key component for the S. pyogenes to form chain like structures[3]. In protein H, the 19 amino-acid sequence (QKQQQLETEKQISEASRKS) that is rich in amines and carboxylic acid side-chains is responsible for homophilic protein-protein interactions that leads to chain like structures. Amines interact with surface Au(0) atoms of the nanoparticles with their lone electron pair with a strength linearly correlating with their basicity corrected for steric hindrance[4]. The kinetics of binding depends on the position of the gold atoms (flat surfaces or edges) while the mode of binding involves a single Au(0) with nitrogen sitting on top of it. A small fraction of surface Au(I) atoms, still present, is reduced by the amines yielding a much stronger Au(0)–RN.+ (RN., after the loss of a proton) interaction. In this case, the mode of binding involves two Au(0) atoms with a bridging nitrogen placed between them. These set of experiments point to the fact that the gold-silver nanodots on top of the silica core of PhaNPs might be disrupting the homophilic interactions of the amine-rich protein H region of *S. pyogenes* which results in their inability to form chains, and disrupts their ability to aggregate before eventually disintegrating the bacteria. The experiment also demonstrated that the PhaNPs also interact with the bacterial membrane and stay attached to it through interactions with thiols, reducing disulfide bridges , and amine clusters by virtue of their noble metal components (Au and Ag) [4, 5].

F. *In vivo* mouse wound model experiments with daily topical dose only.

In vivo mouse wound healing model was created to test the nanoparticle biocompatibility with mouse organism as well as the effectiveness of the PhaNP@Syn71 against *S. pyogenes* wound infection in mice (Main Manuscript Section 3.5). In the first experimental setup, the mice were treated with a daily topical dose of 150 µM PhaNP@Syn71. As controls, Syn71 peptide and Pluronic vehicle were applied. The wound size was measured daily and the results indicate that PhaNP@Syn71 immediately stabilizes the wound and the healing process starts from Day 8 (Figure S4A). By the end of the treatment period (Day 17), the wounds were fully healed by the PhaNP@Syn71. As for the number of mice with wounds, by Day 11, one out of four mice infected had healed, and by Day 15, half of the mice had fully healed by the treatment by PhaNP@Syn71 (Figure S4B). The experiment ended on Day 17, with the wounds fully healed for the treatment group of PhaNP@Syn71 (Figure S4C).

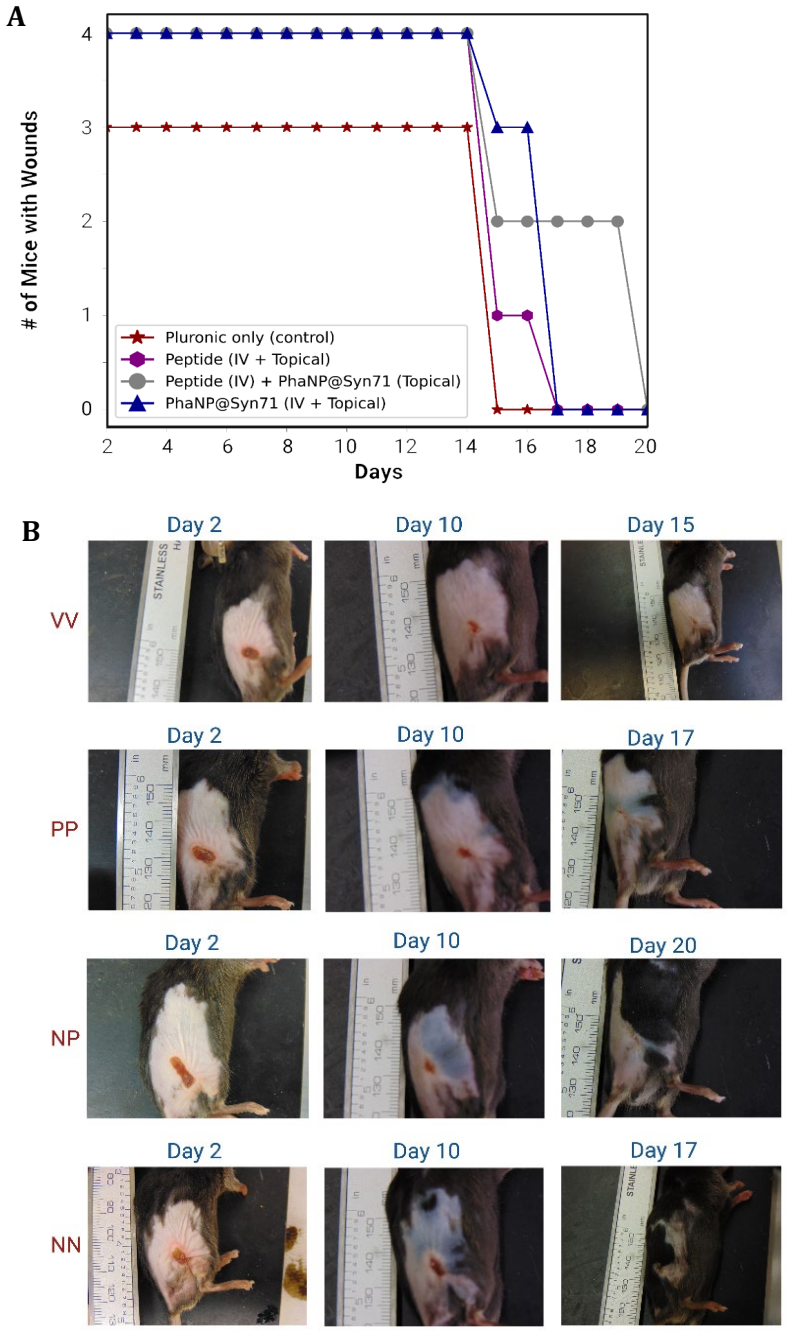

Figure S5 *In vivo* mouse wound model experiments with a combinatory treatment of intravenous (IV) injection followed by a daily topical dose of PhaNP@Syn71. **(A)** Number of mice with wounds throughout the treatment. **(B)** Images of mice wounds at the start of treatment (Day 2), mid-treatment (Day 10) and the end of treatment with Pluronic control (VV =IV+ topical), peptide control (PP=IV + topical), peptide IV + PhaNP@Syn71 topical (NP) and PhaNP@Syn71 (NN= IV + topical)

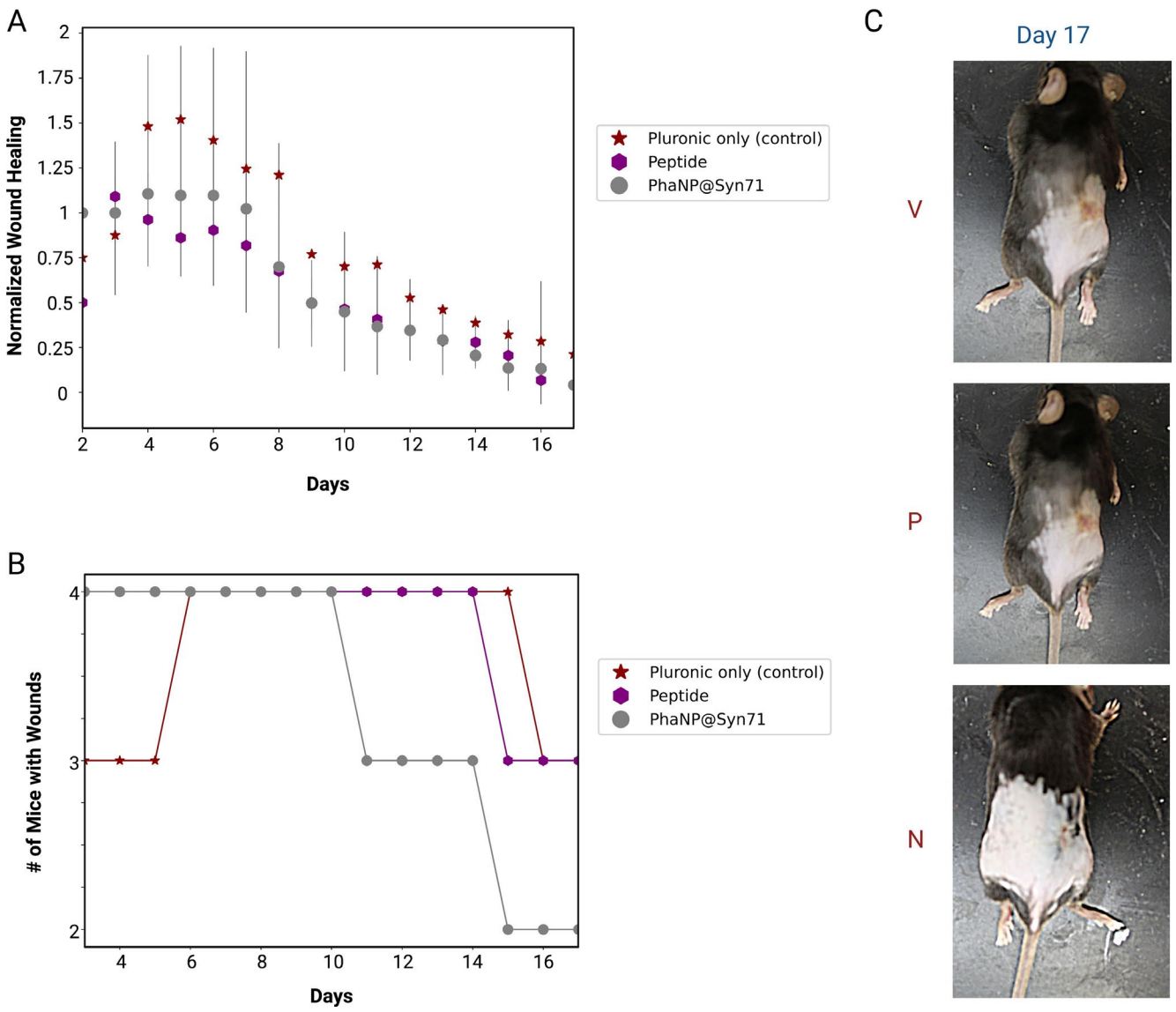

Figure S6 *In vivo* mouse wound model experiments with a treatment of daily topical dose only. **(A)** Normalized wound healing in mice treated with PhaNP@Syn71 vs controls (Pluronic vehicle and Syn71 peptide). **(B)** Number of mice with wounds throughout the treatment. **(C)** Images of mice wounds at the end of treatment (Day 17) with vehicle control (V), peptide control (P) and PhaNP@Syn71 (N).

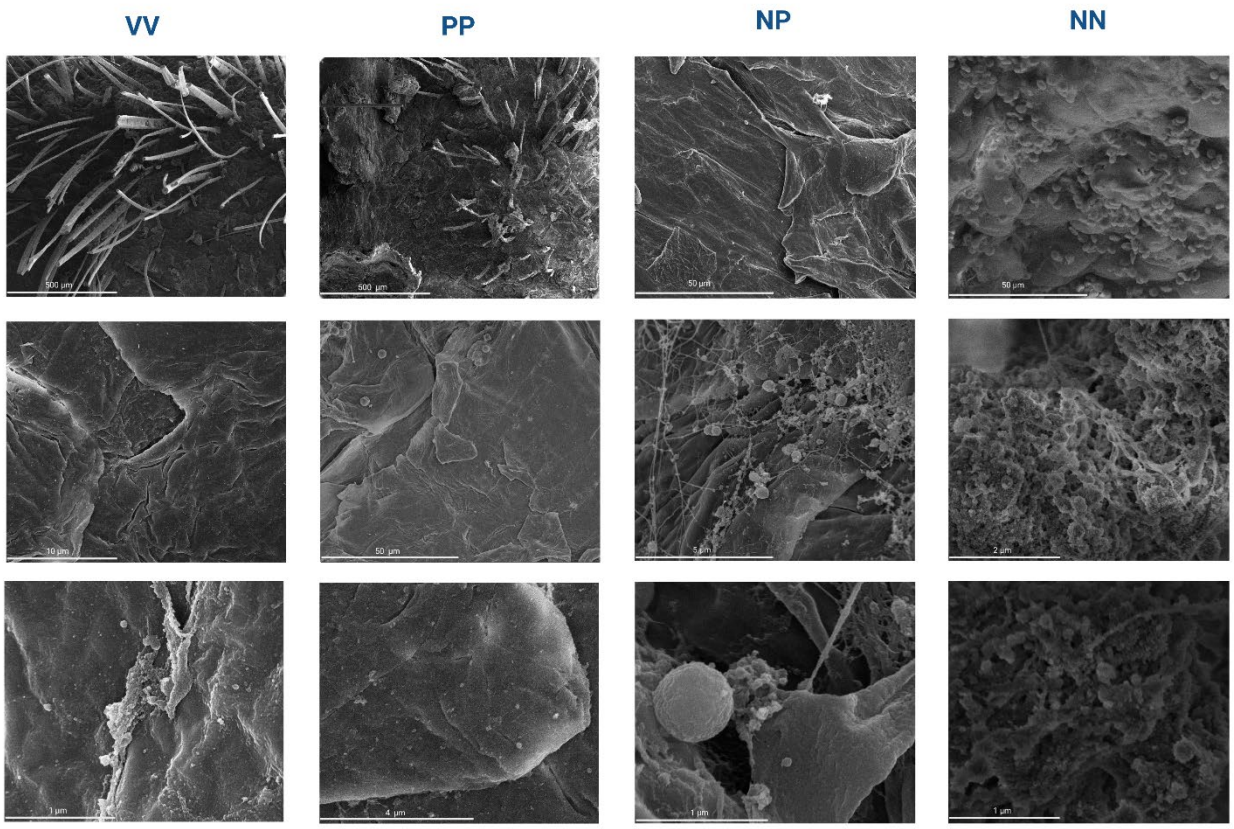

Figure S7 SEM images of the organs and Skin tissue. Skin tissue was inflamed due to normal wound healing process. However, the presence of hair in follicles indicated normal wound healing. Abbreviations: VV - Vehicle (IV + topical), PP - Peptide (IV + Topical), NP - Peptide (IV) + PhaNP@Syn71 (Topical), NN - PhaNP@Syn71 (IV + Topical).

G. ICP-OES analysis on mice organs post-treatment.

ICP-OES analysis of the dissected mouse organs was carried out to determine the amount of PhaNP@Syn71 retained in the organs (Main Manuscript Section 3.5). In any of the treatment variants of one dose of IV + daily topical dose, no Ag was present (Tables S3-S6). There was a slight increase in the amounts of Si and Au for the Peptide IV + Peptide daily topical treatment variant. Higher amounts of Si and Au were observed in treatment variants that incorporated the designed PhaNP@Syn71, either in only IV or in both, IV and daily topical doses. In the case of PhaNP@Syn71 IV + Syn71 peptide daily topical treatment, the most nanoparticles were accumulated in the lungs (Si = 790.977 mg/g of organ, Au = 83.630 mg/g of organ), spleen (Si = 699.298 mg/g of organ, Au = 81.277 mg/g of organ) and large intestines (Si = 679.736 mg/g of organ, Au = 42.55 mg/g of organ) (Table S5). As for the treatment variant of PhaNP@Syn71 IV + PhaNP@Syn71 daily topical dose, the most nanoparticles were retained in the large intestines (Si = 872.651 mg/g of organ, Au = 54.633 mg/g of organ), followed by lungs (Si = 796.975 mg/g of organ, Au = 84.264 mg/g of organ) (Table S6). This allowed us to hypothesize that the nanoparticles are cleared through the GI tract, with the spleen being responsible for the degradation of the nanoparticles. Although more peptides were used in combined IV and daily topical treatment with PhaNP@Syn71 only, the results indicate that in general the nanoparticles were retained more in organs for the treatment where PhaNP@Syn71 was used only in a one-time IV dose.

Table S3 ICP-OES table of mice organs with Vehicle IV + Vehicle topical treatment.

Organ	Au (mg/g of organ)	Si (mg/g of organ)	Ag (mg/g of organ)
Brain	2.815	26.500	-375.436
Large Intestines	8.400	134.180	-1172.141
Heart	6.983	62.031	-940.922
Kidney	3.765	33.781	-511.090
Liver	4.930	39.969	-661.700
Lungs	8.692	82.218	-1164.224
Spleen	9.015	77.567	-1218.405

Table S4 ICP-OES table of mice organs with Peptide IV + Peptide topical treatment.

Organ	Au (mg/g of organ)	Si (mg/g of organ)	Ag (mg/g of organ)
Brain	29.4337	277.080	-3925.390
Large Intestines	57.741	922.294	-8056.741
Heart	62.955	559.175	-8481.819
Kidney	40.903	366.985	-5552.342
Liver	44.121	357.676	-5921.444
Lungs	75.124	710.531	-10061.201
Spleen	106.732	918.306	-14424.447

Table S5 ICP-OES table of mice organs with PhaNP@Syn71 IV + Peptide topical treatment.

Organ	Au (mg/g of organ)	Si (mg/g of organ)	Ag (mg/g of organ)
Brain	57.566	541.911	-7677.240
Large Intestines	42.555	679.736	-5937.868
Heart	60.875	540.697	-8201.529
Kidney	44.314	397.588	-6015.362
Liver	46.501	376.968	-6240.822
Lungs	83.630	790.977	-11200.329
Spleen	81.277	699.298	-10984.346

Table S6 ICP-OES table of mice organs with PhaNP@Syn71 IV + PhaNP@Syn71 topical treatment.

Organ	Au (mg/g of organ)	Si (mg/g of organ)	Ag (mg/g of organ)
Brain	36.524	343.835	-4871.106
Large Intestines	54.633	872.651	-7623.082
Heart	60.013	533.038	-8085.360
Kidney	43.890	393.786	-5957.833
Liver	62.456	506.314	-8382.190
Lungs	84.264	796.975	-11285.264
Spleen	66.155	569.192	-8940.680

H. PhaNP@Syn71 Characterization

The TEM image below actually shows individual silica nanoparticles that are not overlapping or looking fused. Silica unlike Au or Ag is not as electron dense, making it harder to get good image contrast in TEM micrographs of individual nanoparticles. At smaller sizes the NPs exhibit low zeta potential which also contributes to their aggregation during TEM sample prep.

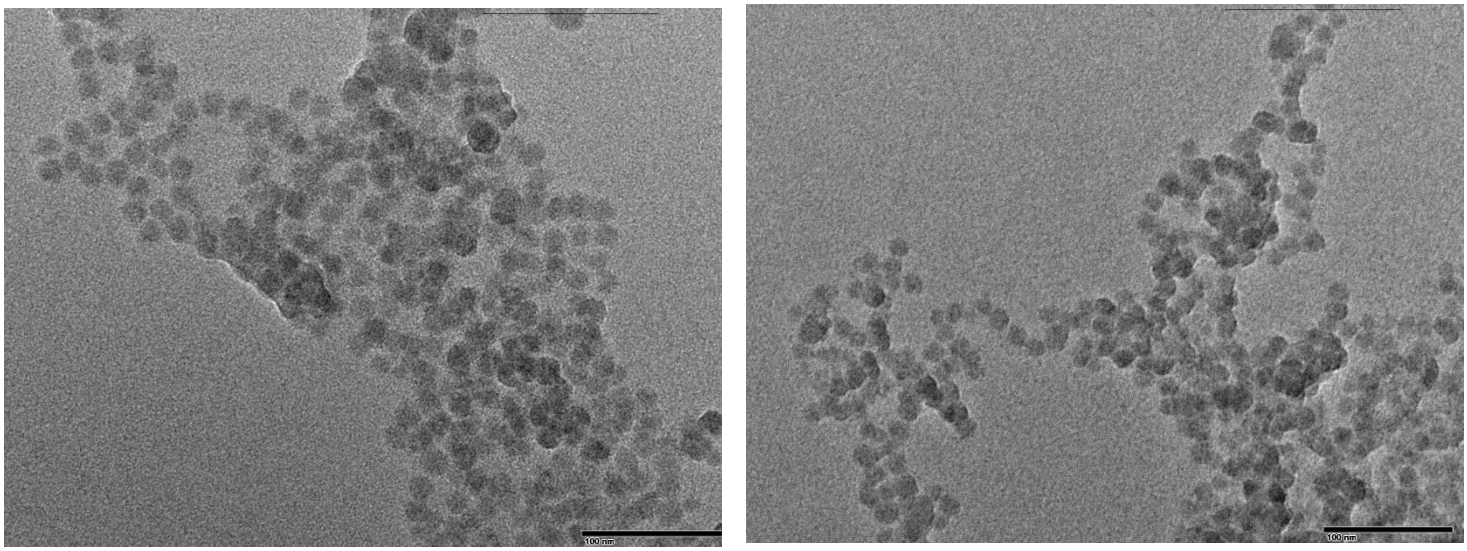

Similarly, TEM micrograph below that shows better contrast of the boundaries of the individual PhaNP@Syn71 even though they are overlapped. The overlapped boundaries with good contrast are bounded by white dash lines to highlight the individual PhaNP@Syn71 nanoparticles

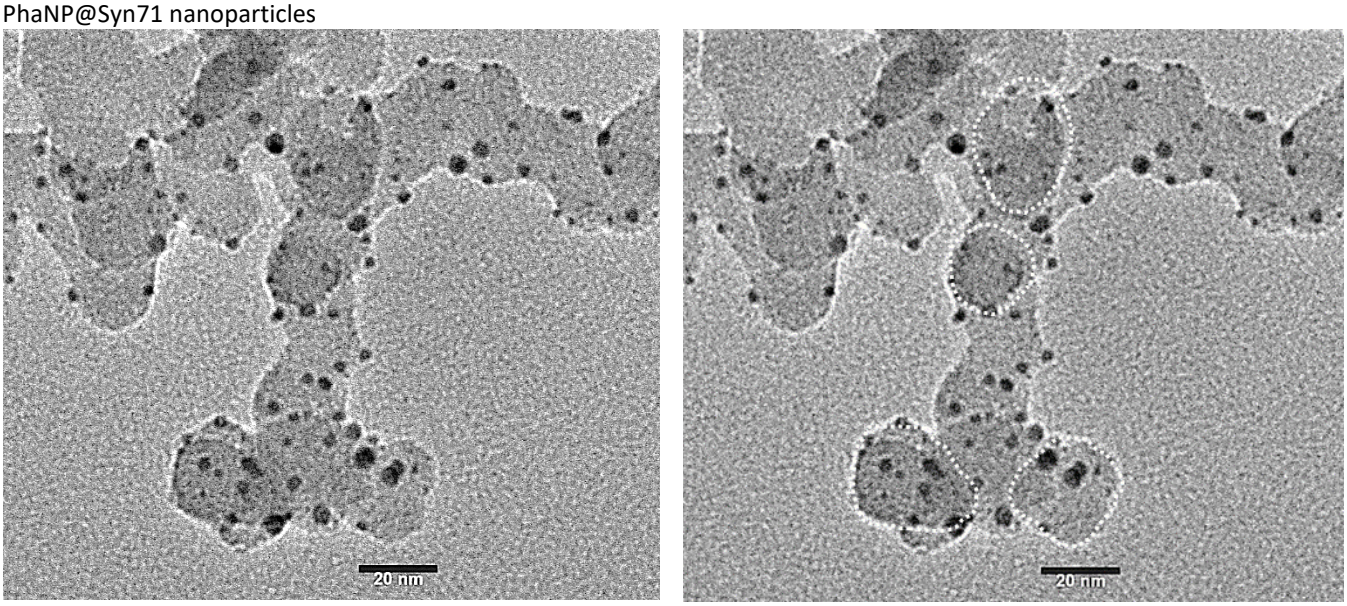

The DLS data discussed in sections 2.3.5 and 3.1 was collected in PBS buffer and therefore the ionic strength of the solvent influences the hydrodynamic radius of nanoparticles. This is not reflective of the true size of the nanoparticles or an indication of aggregation. We have cited the appropriate citations for the correlation between the ionic strength of the solvent and the hydrodynamic radius of nanoparticles with higher ionic strengths contributing to increase in hydrodynamic radius[6, 7, 8].

SEM images of PhaNP (i) and PhaNP@Syn71 (ii) are shown below. The samples were prepped as discussed in section 2.3.2 in the main manuscript. The nanoparticle composition of PhaNPs was further confirmed by SEM images of nanoparticles interaction with *S. pyogenes* as highlighted in iii-v of the figure below. The individual nanoparticle structures with diameters in the range of 20-25 nm can be clearly seen in Figure 4B.ivb,vb and are highlighted by dotted white circles. Similarly, nanoparticle structures in the size range of 20-25 nm can be seen on individual bacteria in figure.iii.b and are highlighted by dotted circles. This indicated that the PhaNPs like structures and the PhaNPs2Syn71 were not aggregating but that they retained their nanoscale dimensions.

(i) PhaNP

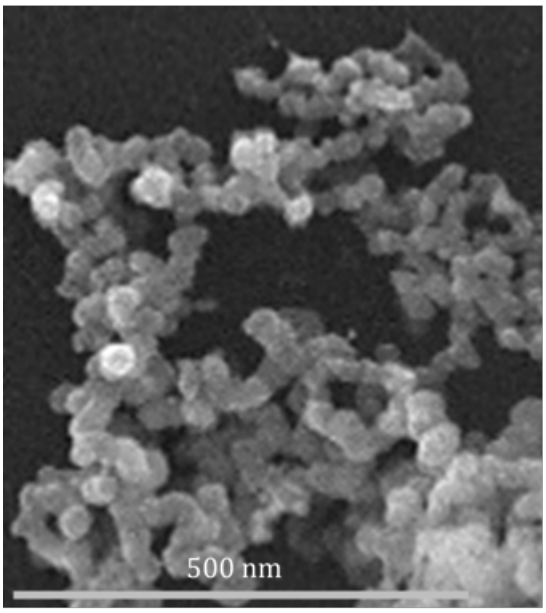

(ii) PhaNP@Syn71

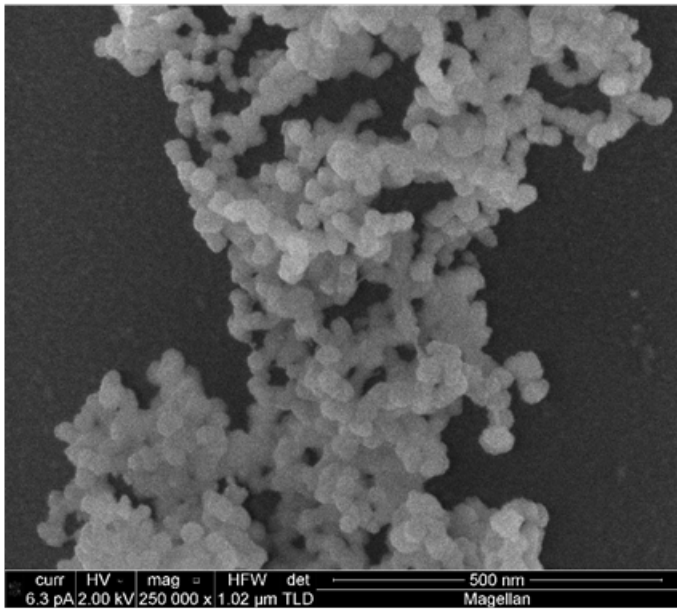

(iii) *S. pyogenes* + SiO_2AuNP

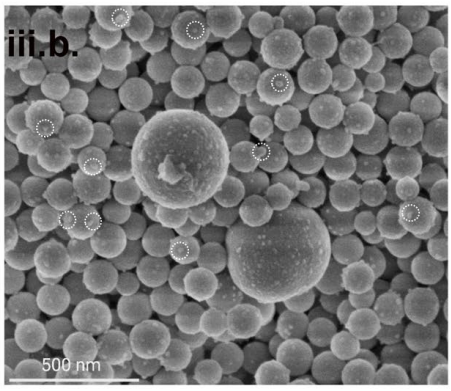

(iv) *S. pyogenes* + PhaNP

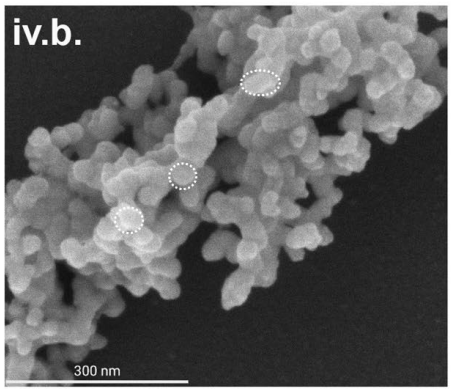

(v) *S. pyogenes* + 25 µM PhaNP@Syn71

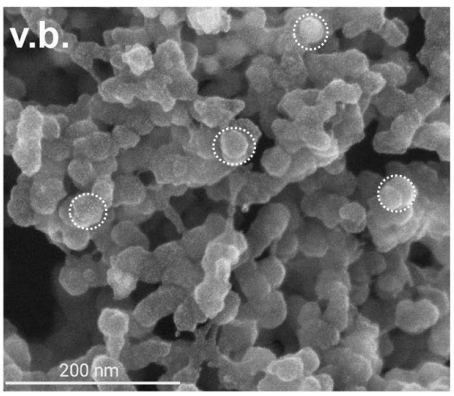

EDXs from SEM image iii.b confirmed the presence of Silica and Au in the sample from the Silica@Au NP. Distinct energy peaks for Si (Kα = 1740 eV), O (Kα = 525 eV), Au (Mα = 2.123 keV, Lα = 9.713 keV) were confirmed in the bacteria samples treated with only SiO_2@Au NPs.

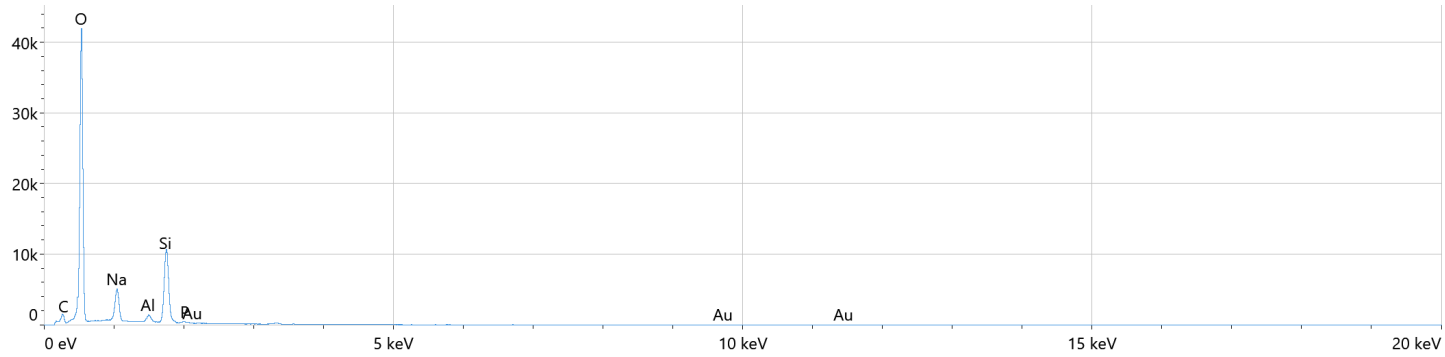

In conclusion, from the TEM results, the SEM images of nanoparticles interaction with the bacteria, the EDXS measurements taken from the SEM images, and from the DLS results we have concluded that we indeed have nanoscale materials with unique antibacterial activity.

References:

1. Wang, W. *et al.* Volume labeling with Alexa Fluor dyes and surface functionalization of highly sensitive fluorescent silica (SiO2) nanoparticles. *Nanoscale* **5**, 10369-10375 (2013).

2. Nallathamby, P.D., Hopf, J., Irimata, L.E., McGinnity, T.L. & Roeder, R.K. Preparation of fluorescent Au-SiO(2) core-shell nanoparticles and nanorods with tunable silica shell thickness and surface modification for immunotargeting. *J Mater Chem B* **4**, 5418-5428 (2016).

3. Frick, I.M., Morgelin, M. & Bjorck, L. Virulent aggregates of Streptococcus pyogenes are generated by homophilic protein-protein interactions. *Mol Microbiol* **37**, 1232-1247 (2000).

4. Lyu, Y. *et al.* The Interaction of Amines with Gold Nanoparticles. *Advanced Materials* (2023).

5. Kim, J. *et al.* Porous gold nanoparticles for attenuating infectivity of influenza A virus. *J Nanobiotechnology* **18**, 54 (2020).

6. McGinnity, T.L. *et al.* Colloidal stability, cytotoxicity, and cellular uptake of HfO2 nanoparticles. *J Biomed Mater Res B Appl Biomater* (2021).

7. Suttiponparnit, K. *et al.* Role of Surface Area, Primary Particle Size, and Crystal Phase on Titanium Dioxide Nanoparticle Dispersion Properties. *Nanoscale Res Lett* **6**, 27 (2010).

8. Nikam, D.S. *et al.* Colloidal stability of polyethylene glycol functionalized Co0.5Zn0.5Fe2O4 nanoparticles: effect of pH, sample and salt concentration for hyperthermia application. *RSC Advances* **4**, 12662-12671 (2014).